Inorg. Chem. **2005**, *44*, 4699–4705

Tuning the Band Gap in Hybrid Tin Iodide Perovskite Semiconductors Using Structural Templating

Jeremy L. Knutson and James D. Martin*

Department of Chemistry, North Carolina State University, Box 8204, Raleigh, North Carolina 27695

David B. Mitzi

IBM T. J. Watson Research Center, P.O. Box 218, Yorktown Heights, New York 10598

Received February 16, 2005

Structural distortions within the extensive family of organic/inorganic hybrid tin iodide perovskite semiconductors are correlated with their experimental exciton energies and calculated band gaps. The extent of the in- and out-of-plane angular distortion of the SnI_4^{2-} perovskite sheets is largely determined by the relative charge density and steric requirements of the organic cations. Variation of the in-plane Sn–I–Sn bond angle was demonstrated to have the greatest impact on the tuning of the band gap, and the equatorial Sn–I bond distances have a significant secondary influence. Extended Hückel tight-binding band calculations are employed to decipher the crystal orbital origins of the structural effects that fine-tune the band structure. The calculations suggest that it may be possible to tune the band gap by as much as 1 eV using the templating influence of the organic cation.

Introduction

Layered perovskites of the form $(R\text{-}NH_3)_2SnI_4$, where R is an organic group, have generated substantial interest recently as a result of the semiconducting character and the potential for high mobility offered by these materials.[1−4] Additionally, the tin(II) iodide-based systems exhibit solubility in a range of common polar solvents, enabling thin-film deposition using solution-based techniques, including spin coating and printing.[5,6] Thin-film field-effect transistors (TFTs), with a spin-coated hybrid perovskite film as the channel layer, have been fabricated by making use of their unusual electrical character and processibility.[5−7] The solution-processed devices have mobilities in the range of amorphous silicon ($\sim$1 $cm^2\ V^{-1}\ s^{-1}$), but the processing is performed entirely at near-ambient temperature. Higher mobilities have also been achieved using low-temperature melt-processed hybrid films (as high as 2.6 $cm^2\ V^{-1}\ s^{-1}$ in the saturation regime),[8] presumably as a result of the better grain structure relative to the solution-processed films. The key to the electronic application of the hybrid semiconductors is the ability to conveniently tailor the electronic properties. The band gap is a particularly important characteristic because it relates to the ability to inject charge and influence the carrier density in the material at a given temperature as well as to determine the wavelength of light that might be emitted under electrical or optical stimulation.

Structurally, the layered perovskites consist of sheets of corner-sharing tin(II) iodide octahedra separated by layers of organic cations (generally organic ammonium cations).[9] For simple organic cations (i.e., those with large HOMO−LUMO separation), the Sn and I states dominate the electronic character of the valence and conduction bands yielding a direct band gap.[4] The exciton-binding energy in the layered hybrids is unusually large as a result of the low-dimensional nature of the solid as well as the small effective

* To whom correspondence should be addressed. E-mail: JDMARTIN@NCSU.EDU.

(1) Mitzi, D. B.; Feild, C. A.; Harrison, W. T. A.; Guloy, A. M. *Nature* **1994**, *369*, 467.
(2) Mitzi, D. B.; Wang, S.; Feild, C. A.; Chess, C. A.; Guloy, A. M. *Science* **1995**, *267*, 1473.
(3) (a) Mitzi, D. B.; Feild, C. A.; Schlesinger, Z.; Laibowitz, R. B. *J. Solid State Chem.* **1995**, *114*, 159. (b) Mitzi, D. B.; Liang, K. *J. Solid State Chem.* **1997**, *134*, 376.
(4) Papavassiliou, G. C.; Koutselas, I. B.; Terzis, A.; Whangbo, M.-H. *Solid State Commun.* **1994**, *91*, 695.
(5) Kagan, C. R.; Mitzi, D. B.; Dimitrakopoulos, C. D. *Science* **1999**, *286*, 945.
(6) Mitzi, D. B.; Chondroudis, K.; Kagan, C. R. *IBM J. Res. Dev.* **2001**, *45*, 29.
(7) Mitzi, D. B.; Dimitrakopoulos, C. D.; Kosbar, L. L. *Chem. Mater.* **2001**, *13*, 3728.
(8) Mitzi, D. B.; Dimitrakopoulos, C. D.; Rosner, J.; Medeiros, D. R.; Xu, Z.; Noyan, C. *Adv. Mater.* **2002**, *14*, 1772.
(9) Mitzi, D. *Prog. Inorg. Chem.* **1999**, *48*, 1−121.

10.1021/ic050244q CCC: $30.25
Published on Web 05/25/2005

Table 1. Electronic and Structural Parameters for a Series of $[RNH_3]_2SnI_4$ Hybrid Perovskite Semiconductors

	amine (RNH_2)	exciton energy (eV, nm)	Sn−I−Sn bond angle (deg)[m]	in-/out-of-plane distortion (deg)[m]	eq/ax Sn−I bond length (Å)[m]	distortion of SnI_6 octahedron[n]	cation penetration (Å)[o]
1	4-ClPEA[b,k]	2.02, 615	157.0	22.9/<1	3.139/3.176	0.017	0.58
2	PEA[a]	2.04, 609	156.5	23.5/<1	3.136/3.161	0.012	0.57
3[l]	4-FPEA[b]	2.04, 609	156.4	23.7/<1	3.135/3.181	0.020	0.56
4	NEA[c,k]	2.06, 602	156.6	23.4/<1	3.152/3.204	0.023	0.58
5	3-FPEA[b]	2.07, 599	154.2	25.8/<1	3.136/3.207	0.033	0.57
6	N5FPEA[d]	2.11, 588	154.5	25.5/<1	3.161/3.184	0.020	0.51
7	2-FPEA[b]	2.11, 588	153.3	26.7/<1	3.149/3.178	0.013	0.47
8[l]	2-ClPEA[b]	2.12, 586	154.8	25.2/<1	3.169/3.156	0.006	0.48
9	5FPEA[f,k]	2.17, 572	152.4	27.6/<1	3.169/3.173	0.041	0.46
10[l]	2-BrPEA[b]	2.23, 557	148.7	25.1/11.3	3.145/3.155	0.005	0.37
11[l]	2-CF_3PEA[g,k]	2.23, 556	149.6	23.2/12.3	3.147/3.162	0.007	0.40
12[l]	1-PYREA[e,k]	2.28, 545	144.1	28.5/12.3	3.124/3.170	0.020	0.28
13[l]	*n*-buA[h]	2.04, 607	159.6	19.4/6.4	3.136/3.160	0.011	0.76
14	*n*-dodecylA[i]	2.14, 580	155.7	16.7/11.2	3.138/3.152	0.007	0.52
15[l]	TMAEA[j]	1.97, 630	166.9	0.8/11.8	3.162/3.127	0.015	0.99/−1.22

[a] Phenethylamine (see refs 4 and 7). [b] Halogen-substituted phenethylamine (on the *m* position of the phenyl ring), abbreviated as *m*-XPEA; $m = 4$, 3, or 2 and X = F, Cl, or Br (see refs 7 and 13). [c] 2-Naphthaleneethylamine (see ref 13). [d] Mixture of 2-naphthaleneethylamine and pentafluorophenethylamine (1:1) (see ref 14). [e] 1-Pyreneethylamine (see ref 13). [f] Pentafluorophenethylamine (see ref 14). [g] 2-Trifluoromethylphenethylamine. [h] *n*-Butylamine (see ref 12). [i] *n*-Dodecylamine (see ref 21). [j] 2-Trimethylammonioethylamine (see ref 20). [k] Unpublished crystal structures. [l] A structure for which the band structure was calculated from the crystallographic coordinates. [m] Values represent averages for each structure. [n] Bond length distortion is defined as $\sum \mathrm{abs}(d_i - \langle d \rangle)/6$, where d_i is the summation over the six Sn−I distances and $\langle d \rangle$ represents the average bond length. [o] Cation penetration is defined by the distance between the planes of the N atoms of the cation and the planes of the axial I atoms of the perovskite sheet.

dielectric constant that results from the organic layers sandwiching the active inorganic sheets.[10] For $(C_6H_5CH_2CH_2NH_3)_2SnI_4$, the binding energy is on the order of 0.19 eV,[4] which is large compared to k_BT at room temperature. While the band gap of the hybrid can be tailored by making substitutions on the metal or halogen sites of the hybrid structures,[11,12] these substitutions invariably introduce disorder into the semiconducting component of the structure, thereby likely adversely affecting the mobility. Recently, steric hindrance and other structural effects from the organic component have been used to indirectly impact the detailed structure of the inorganic framework and consequently the wavelength of the exciton peak in the absorption spectrum, with an associated shift in the band gap, over a fairly wide range.[7,13,14] It was proposed that this shift in the band gap may be correlated to a shift in the Sn−I−Sn bond angle between adjacent octahedra, away from the ideal (undistorted) value of 180°. In an effort to elucidate the crystal orbital basis for the variation in the band gap, extended Hückel tight-binding band calculations were performed on a series of SnI_4^{2-} perovskite-type structures to determine the impact on the electrical properties of the bonding interactions reflected by the Sn−I−Sn bond angle and the Sn−I distance.

Experimental Section

Extended Hückel tight-binding band structure calculations were performed using the CAESAR suite of programs.[15] Although this method typically underestimates the band gap, the extended Hückel technique is very reliable for describing structure−property trends.[16] Calculations were performed on a series of idealized undistorted and distorted 2D perovskite lattices as well as on lattices using coordinates from single-crystal structures. Idealized structures were calculated with Sn−I distances of 3.14 and 3.16 Å, consistent with the range of average distances determined from the crystal structures. The two bonding distances were employed to explore the effect of bond length on electronic properties. The extent of angular distortion is indicated by the deviation of the Sn−I−Sn angle α from the ideal 180° (Figure 1a). The observed structures indicate deviations that occur as an entirely in-plane distortion as shown in Figure 1b, an entirely out-of-plane distortion along one axis as shown in Figure 1c, or a combination of in- and out-of-plane distortions resulting in the puckered lattice shown in Figure 1d. In all of the distortions considered, the tin atoms remain coplanar. The in-plane and out-of-plane contributions to the bond angle distortions (given in Table 1 for the experimental single-

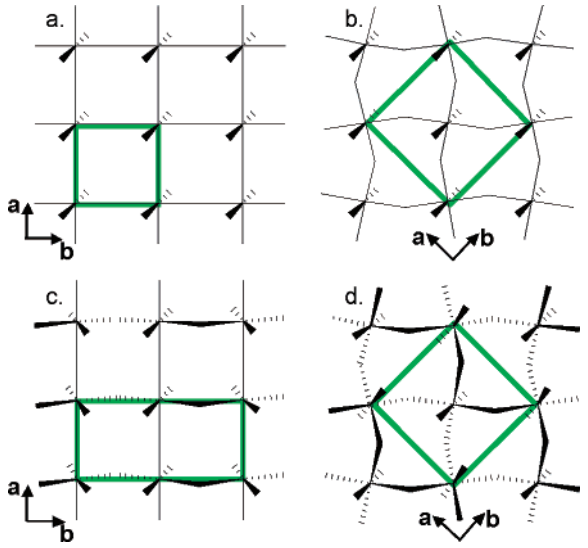

Figure 1. Schematic of 2D perovskite sheets which shows the (a) undistorted lattice, (b) in-plane distortion, (c) out-of-plane distortion, and (d) combined in- and out-of plane distortion. The green box highlights the unit cell that describes each lattice.

(10) Hong, X.; Ishihara, T.; Nurmikko, A. V. *Phys. Rev. B* **1992**, *45*, 6961.
(11) Papavassiliou, G. C.; Koutselas, I. B. *Synth. Met.* **1995**, *71*, 1713.
(12) Mitzi, D. B. *Chem. Mater.* **1996**, *8*, 791.
(13) Xu, Z.; Mitzi, D. B.; Dimitrakopoulos, C. D.; Maxcy, K. R. *Inorg. Chem.* **2003**, *42*, 2031.
(14) Xu, Z.; Mitzi, D. B. *Chem. Mater.* **2003**, *15*, 3632.
(15) Ren, J.; Liang, W.; Whangbo, M.-H. *Crystal and Electronic Structure Analysis Using CAESAR*; PrimeColor Software: Raleigh, NC, 1998, www.primec.com.
(16) Whangbo, M.-H. *Theor. Chem. Acc.* **2000**, *103*, 252.

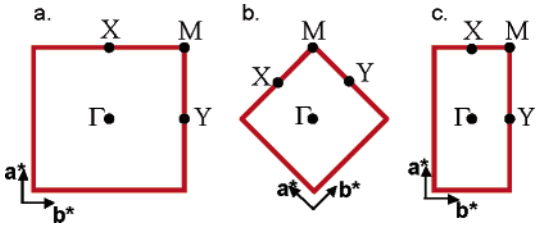

Figure 2. Representations of the first Brillion Zone for (a) the ideal undistorted unit cell, (b) the $\sqrt{2} \times \sqrt{2}$ unit cell, and (c) the 1×2 unit cells described in Figure 1. The size of each reciprocal lattice drawn is scaled relative to the undistorted lattice. $\Gamma = 0, 0$; $X = a^*/2, 0$; $Y = 0, b^*/2$; and $M = a^*/2, b^*/2$.

crystal structures) were determined by the projection of the equatorial (bridging) iodine atoms onto the plane of tin atoms and the deviation of the axial (terminal) Sn−I bonds from the normal to the plane of tin atoms, respectively. Different unit cells are required to describe each type of distortion. The different size and orientation of the unit cell with respect to the perovskite lattice require the evaluation of different reciprocal space vectors in the first Brillion zone. For example, to determine the band dispersion along the corner-shared octahedral chains, it is necessary to evaluate the reciprocal-space line segment from Γ to *X* (Figure 2a) for the undistorted lattice (Figure 1a) but the line segment from Γ to *M* (Figure 2b) for the in-plane distorted lattice (Figure 1b). Similarly, whereas the square lattices of the structures represented by panels a, b, and d of Figure 1 have identical dispersions along the *a** and *b** directions, the rectangular lattice of the out-of-plane distortion (Figure 1c) requires independent calculation of the dispersion along *a** and *b**.

Results and Discussion

Band Structure. To understand the electronic structure in these hybrid layered perovskite materials, we begin with a systematic description of the band structure. The band structure calculated for the observed distorted structure of $(C_6H_5CH_2CH_2NH_3)_2SnI_4$ was previously reported using a large $(SnI_4^{2-})_4$ unit cell.[4] However, to more clearly describe the orbital origins of the $(SnI_4^{2-})_n$ band structure and its distortions, it is helpful to first consider the band structure of the idealized undistorted lattice shown in Figure 1a. Our orbital-based analysis of the electronic structure of these main-group halide perovskites is very similar to the analysis described by Canadell and Whangbo for low-dimensional transition metal oxide perovskites.[17] Instead of π^* interactions between the transition metal d orbitals and the oxygen p orbitals, dispersion in these main-group halides will originate from σ^* interactions between the main-group metal and iodine p orbitals. Similar dispersion characteristics are evident in the recent analysis of the 3D tin oxide perovskites.[18] As described previously,[4] because of the large separation between SnI_4^{2-} sheets by the alkylammonium cations, it is only necessary to consider the band structure of a single 2D sheet. Furthermore, since the alkylammonium cations do not significantly participate in the frontier orbitals, the system can be further simplified by considering only the inorganic lattice.

In the +2 oxidation state, the highest-occupied orbitals will be localized on the Sn 5s orbitals, and thus, these orbitals

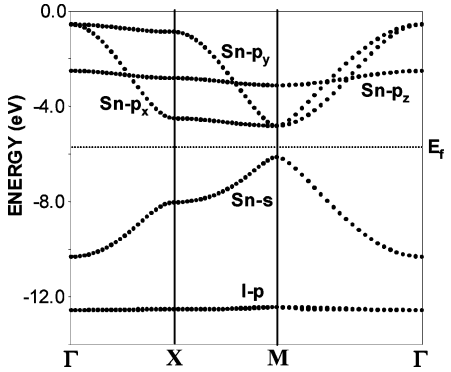

Figure 3. Calculated band structure for an idealized undistorted SnI_4^{2-} perovskite sheet showing the bands on either side of the Fermi level, E_f. $\Gamma = 0, 0$; $X = a^*/2, 0$; $M = a^*/2, b^*/2$.

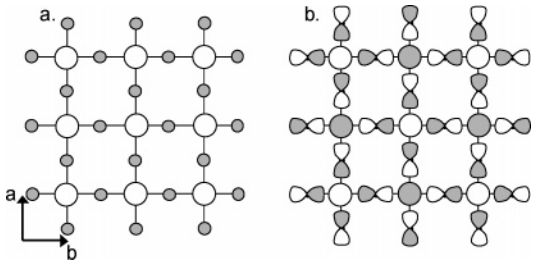

Figure 4. Representation of the crystal orbitals of the valence band at (a) Γ and (b) *M* for an ideal undistorted SnI_4^{2-} perovskite layer.

are the origin of the valence band of the extended lattice. The lowest-unoccupied orbitals, localized on the Sn 5p orbitals, are the origin of the conduction bands. In an octahedral SnI_6 molecular fragment, both the Sn s and p orbitals will be destabilized by σ-antibonding interactions with the iodine 5p and 5s orbitals. However, in the infinite lattice of the perovskite sheet, the extent of the Sn−I antibonding interaction is determined by the location in reciprocal space, thus giving rise to the dispersion of the band structure.

The calculated band structure for an idealized undistorted 2D SnI_4^{2-} perovskite sheet is given in Figure 3. The Sn 5s-based valence band is at its lowest energy at Γ where the s orbitals on all of the tin centers in the 2D lattice are in phase. At this point, symmetry prevents I p_x and p_y orbitals from mixing with the Sn 5s orbitals, as represented in Figure 4a, although some antibonding with the I s orbitals is observed. Along the reciprocal space vectors *a** and *b**, the I p_x and p_y orbitals begin to mix with the Sn s orbitals in a σ-antibonding fashion, with the maximum destabilization being observed at the reciprocal lattice point *M*, as represented in Figure 4b. The antibonding interactions between the Sn s orbitals and I p_z orbitals, oriented orthogonal to the perovskite plane, are effectively constant across all of the reciprocal space. Nevertheless, with strong dispersion in both the *a** and *b** directions, the valence band is clearly two dimensional.

The conduction bands derived from the Sn 5p orbitals exhibit much more distinct directional characteristics. The band derived from the Sn p_z orbitals shows effectively no

(17) Canadell, E.; Whangbo, M.-H. *Chem. Rev.* **1991**, *91*, 965−1034.

(18) Mizoguchi, H.; Eng, H. W.; Woodward, P. M. *Inorg. Chem.* **2004**, *43*, 1667.

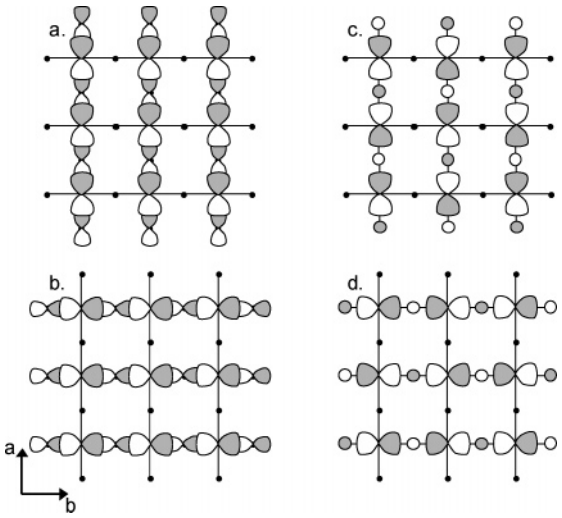

Figure 5. Representation of the degenerate crystal orbitals for an ideal undistorted unit cell derived from the Sn p_x and p_y orbitals (conduction band) at Γ (a and b) and at *M* (c and d).

dispersion in the 2D perovskite because the alkylammonium cations separate tin iodide layers in the *c* direction and the π-type Sn−I interactions in the *ab* plane are very weak. Each of the Sn p_x and p_y bands exhibits significant dispersion where strong σ-antibonding interactions with the iodine p_x and p_y orbitals are observed at Γ, as shown in Figure 5, and much weaker antibonding interactions with the I s orbitals are possible at *M*. Unlike the 2D Sn s-based valence band, the conduction p_x band is dispersive only in the *a** direction (Γ to *X* in Figure 3), and the p_y band is dispersive only in the *b** direction (*X* to *M* in Figure 3). Thus, the conduction bands of these perovskite materials consist of two superimposed 1D bands.

The occurrence of the maximum destabilization of the valence band and the maximum stabilization of the conduction band at the same point in reciprocal space makes the tin iodide perovskites direct band gap semiconductors. Interestingly, it has been reported that these tin iodide semiconductors are preferentially p-doped, partially removing electrons from the valence band.[3] On the basis of an understanding of the band structure, superior conductivity is predicted when a two-dimensional Fermi surface is created by partially oxidizing (p-doping) the 2D valence band, as opposed to a partial reduction (n-doping) of the pseudo-1D conduction bands, which are much more susceptible to electronic instability.

Structural Distortions and the Band Gap. The basic structural motif of corner-sharing octahedra is common to all of the hybrid perovskite materials. However, the charge density, shape, and functionalization of the templating cation have a significant impact on subtle structural distortions of the tin iodide lattice.[7,9,13,14,19] The small ammonium headgroup, common to most of the tin iodide hybrid salts prepared to date, has a higher charge density than is required by an ideal SnI_4^{2-} lattice. As a result, the system most commonly distorts with the in-plane-type distortion shown in Figure 1b and Table 1. Decreasing the Sn−I−Sn bond angle to about 155° with in-plane distortion brings the tin octahedra into closer proximity, thus increasing the charge density of the anionic inorganic layer. By contrast, the significantly more sterically demanding trimethylammonium cationic headgroup is too large to accommodate the charge density requirements of an undistorted perovskite lattice. However, the bis-cation $[Me_3NCH_2CH_2NH_3]^{2+}$, TMAEA, links a high- and low-charge density cation to either end of the bis-cation, which together have been shown to accommodate a SnI_4^{2-}-layered perovskite structure.[20] The large trimethylammonium headgroup requires an out-of-plane distortion to the perovskite sheet, similar to that described in Figure 1c, effectively lowering the charge density about one face of a Sn_4I_{16} perovskite square. At the same time, this out-of-plane distortion also forms a higher-charge density face on the opposite side, which is charge balanced by the smaller ammonium cationic headgroup. Furthermore, when considerable bulkiness is added to the organic tail of the templating cation, such as in the 2-BrPEA, 2-CF_3PEA, and 1-PYREA salts, or when the organic tails are interdigitated, such as in *n*-dodecylA and *n*-buA salts (only marginally interdigitated in the latter case), a combination of in-plane and out-of-plane distortions are observed.

Interestingly, there appears to be a correlation between the subtle variation in these angular distortions and the materials band gap as observed with UV−vis spectroscopy.[7,13,14] This is demonstrated by comparison of the energy (wavelength) of the observed exciton peak with the respective Sn−I−Sn bond angles for a series of hybrid tin iodide perovskite materials, given in Table 1. Note that, by comparison, there is little to no global correlation between the average Sn−I bond length and the energy of the exciton peak. We again turn to a series of band structure calculations to understand the impact of the subtle angular distortions on the electronic structure of these perovskite semiconductors. The distortions of the crystalline lattice require an expanded unit cell which, in turn, results in a folding of the band structure and thus a change in the reciprocal space point at which the direct band gap is observed. As a point of reference, the band structure reported by Papavassiliou et al.[4] for the $(SnI_4^{2-})_4$ unit cell is folded four times, with respect to the band structure plot in Figure 3 for the (SnI_4^{2-}) unit cell. Nevertheless, the overall picture of the impact of the distortion on the band gap is readily understood from the perturbation to the orbital descriptions presented above for the ideal lattice.

In-Plane Distortions. Because the periodic propagation of the 2D perovskite network is within the *ab* plane, in-plane distortions have a more drastic impact on the band gap than exclusively out-of-plane distortions. The impact of the distortion on the energies of the valence and conduction bands at the band gap is plotted in Figure 6. Bending the Sn−I−Sn bond angle away from 180°, where maximal orbital overlap is achieved, results in a loss of antibonding interactions between the Sn s orbitals and the I p_x and p_y

(19) Martin, J. D.; Yang, J.; Dattelbaum, A. M. *Chem. Mater.* **2001**, *13*, 392−399.

(20) Xu, Z.; Mitzi, D. B.; Medeiros, D. R. *Inorg. Chem.* **2003**, *42*, 1400−1402.

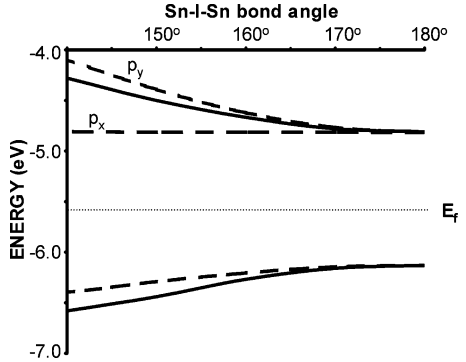

Figure 6. Plot of the energy of the top of the valence band (Sn s-based) and bottom of the conduction bands (Sn p_x- and p_y-based) upon in-plane (solid lines) and out-of-plane (dashed lines) distortions to the SnI_4^{2-} perovskite lattice (calculated with an average Sn−I distance of 3.16 Å) which demonstrates the origin of the band gap variation with structural distortion. The Fermi energy is marked by a dotted line.

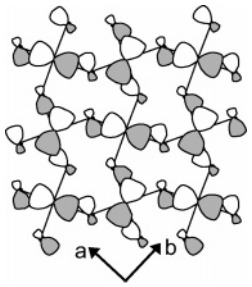

Figure 7. Representation of one member of the set of degenerate crystal orbitals at Γ ($\sqrt{2} \times \sqrt{2}$ unit cell), the lowest energy point of the conduction band, as calculated for the 140° in-plane distortion.

orbitals, thus lowering the top of the valence band (i.e., distortion results in a loss of antibonding from the crystal orbital shown in Figure 4b). A similar effect results in the lowering of the top of the conduction bands (Figure 5a, b) as antibonding interactions between Sn p and I p orbitals are lost upon distortion. While this diminishes the dispersion of the conduction band, the bottom of the conduction band determines the band gap, which is largely nonbonding in the idealized structure (Figure 5c, d). However, in-plane distortion lowers the symmetry of the lattice so that I p_x and p_y character mix into these crystal orbitals as well, resulting in significant antibonding between the Sn p and I s/p hybrid orbitals in the conduction band, as shown in Figure 7 for one member of the degenerate pair of crystal orbitals at Γ. This orbital mixing, caused by lowered symmetry, raises the energy of the bottom of the conduction band (Figure 6) and is in part responsible for the increased band gap upon distortion. Along with the decreased width of the conduction bands, the orbital mixing from symmetry lowering diminishes the pseudo-1D character of the Sn p_x and p_y bands. The extent to which the I s/p orbitals are mixed into the bottom of the conduction band is directly related to the increased distortion of the Sn−I−Sn bond angle.

Out-of-Plane Distortions. Geometrically, it is only possible to create an exclusively out-of-plane distortion of a 2D perovskite-type lattice in one direction at a time. Simultaneous out-of-plane distortion along the *a* and *b* directions requires both an in-plane and out-of-plane component to the distortion. This, of course, has a significant impact on the electronic structure. Calculations were performed on the series of idealized out-of-plane distortions created by twisting corner-sharing octahedral chains running along the *a* direction as represented in Figure 1c. The bonding interactions running along the axis of the twist are effectively unperturbed by the distortion. This is most clearly observed in the band derived from the Sn p_x orbitals (crystal orbitals in Figure 5a, c) for which the bottom of the conduction band is unchanged by distortion (Figure 6). By contrast, bending the Sn−I−Sn angle along the *b* direction lowers the lattice symmetry so that the I p_y and p_z orbitals can now mix with I s character, creating significant antibonding interactions between the Sn p and I s/p hybrid orbitals. This destabilization of the p_y band caused by the out-of-plane distortion in the *bc* plane is similar to that observed for both the p_x and p_y bands described above for the in-plane distortions within the *ab* plane. This out-of-plane distortion thus separates the two pseudo-1D conduction bands (Figure 6). The top of the Sn s-based valence band is stabilized by the out-of-plane distortion because of the loss of the Sn−I overlap upon distortion away from the ideal 180°. However, because the out-of-plane angular distortion is only along one direction, the stabilization of the valence band upon distortion is only about half that observed for the in-plane distortion, as shown in Figure 6.

Sn−I Bond Distances. The SnI_6 octahedra in these hybrid perovskite structures exhibit a range of structural distortions in their Sn−I distances, as described in Table 1. The 5FPEA salt exhibits the greatest distortion with individual Sn−I distances ranging from 3.104 to 3.233 Å, and the 2-BrPEA salt exhibits the most ideal octahedron with individual distances ranging from 3.141 to 3.155 Å. The axial Sn−I distances determine the energy of the flat Sn p_z band but have no direct impact on the band gap. However, variation in the equatorial Sn−I distances has a modest impact on the material's band gap. Calculations were performed for the in-plane and out-of plane distortions of a 2D perovskite lattice of ideal octahedra with average Sn−I distances of 3.14 and 3.16 Å. These data are summarized in Figure 8. Shorter Sn−I distances result in a destabilization of the top of the valence band because of increased Sn−I antibonding, while the nonbonding crystal orbitals of the bottom of the conduction band are not significantly affected by variation of the Sn−I distances.

Comparison To Experiment

A plot of the energy of the observed exciton peaks as a function of the Sn−I−Sn bond angle is also shown in Figure 8. The exciton energy is a reasonable approximation of the band gap, although, in fact, it is a few hundred millielectronvolts lower than that of the band gap.[4] The band gap was calculated for a series of seven of the experimental structures, indicated in Table 1, for which the coordinates of the $(SnI_4^{2-})_n$ sheet were taken directly from the single-crystal structures. The trends in the calculated band gaps are in good agreement with the experimental UV−vis spectroscopic measurement of the exciton energy. As noted above, the band-gap energies, calculated by the extended Hückel

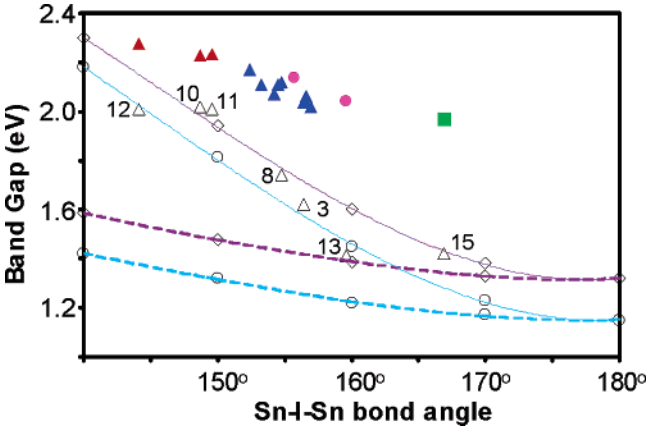

Figure 8. Plot of the calculated band gap as a function of the in-plane (solid lines) and out-of-plane (dashed lines) distortions. Purple and blue lines represent calculations with average Sn−I distances of 3.16 and 3.14 Å, respectively. Open circles and diamonds represent calculated band gaps for idealized structures with Sn−I distances of 3.14 and 3.16 Å, respectively; open triangles represent calculated band gaps for experimental crystal structures (reference numbers are correlated with Table 1). Filled symbols represent the experimental exciton peak energies from Table 1 for the following systems: blue triangles for purely in-plane distortion and red triangles for combined in- and out-of-plane distortions (PEA derivatives **1**−**12**), purple circles for alkylammonium derivatives **13** and **14**, and green squares for TMAEA **15**.

method, are frequently below the actual energy of the band gap[16] (here they are off by a factor of about 1.2). Most importantly, however, the calculated band structures of the experimental structures are consistent with the bond-angle and bond-distance trends described above on the basis of idealized structures, as summarized in Figure 8.

Both calculated and spectroscopic data demonstrate that the Sn−I−Sn bond angle is the dominant structural factor that controls the variation in the band gap. For example, it is the significantly different Sn−I−Sn bond angle (Δ = 12.9°), not the nearly identical equatorial Sn−I distances (Δ = 0.016 Å), which determines the difference in exciton energies between the arylammonium-templated compounds **1** and **12** (Δ = 0.26 eV). Nevertheless, compounds **5**, **6**, and **8** exhibit nearly identical Sn−I−Sn bond angles (154.5 ± 0.3°), yet their exciton energies differ by 0.05 eV. This smaller difference in the exciton energies of compounds **5**, **6**, and **8**, however, correlates linearly with the average equatorial Sn−I bond distance (the shorter Sn−I bond distance corresponding to the lowest exciton energy as suggested by the calculations). The phenylethylammonium (PEA)-templated salts **1**−**9**, in which there is no significant out-of-plane distortion, are completely consistent with these Sn−I−Sn bond-angle and equatorial Sn−I bond-distance arguments. Compound **15** is the closest example of an exclusively out-of-plane distortion, and its calculated band gap lies just above the out-of plane trend line, as is expected for the combination of in- and out-of-plane distortions. Unfortunately, there are not more examples of primarily out-of-plane distorted structures to provide stronger support for the observation that the out-of-plane distortions retain the smallest band gaps. Compounds **10**−**12**, which exhibit significant in-plane and out-of plane distortions, largely track the in-plane trends because the combined distortion does not retain a lattice direction with the nondistorted (Sn−I−Sn = 180°) contacts that ensured broad dispersion of the conduction band as described above for an exclusively out-of-plane distortion.

Thus far, our analysis has ignored any direct influence (other than structure directing) for the templating cations with respect to the electronic properties of the hybrids. Interestingly, however, both the butylammonium- and dodecylammonium-templated compounds (compounds **13** and **14**, respectively) exhibit a higher exciton energy than that observed for arylammonium-templated compounds with similar metrical parameters. The calculated band gap for compound **13**, based on only the SnI_4^{2-} part of the crystal structure, is consistent with the experimental bond-angle distortion with a diminished band gap because of the short equatorial Sn−I distances. However, this compound exhibits the greatest difference between the calculated band gap and the observed exciton energy of any of the compounds examined. It has been suggested that the lower dielectric constants of the alkylammonium cations should yield exciton-binding energies approximately 0.1 eV larger than that of the arylammonium cations (and thus lower exciton energies).[10] However, the band gap may be increased to an even greater extent as a result of a larger electrostatic energy,[22] for the systems with the lower dielectric constant barrier layers, thereby potentially leading to a larger overall exciton energy (as measured by optical absorption experiments, for example). An alternative explanation for this shift in exciton energies to higher values may involve the extent to which the templating cation penetrates into the perovskite sheet. Hydrogen bonding between the ammonium head and both axial and equatorial iodide atoms of the perovskite network has previously been noted,[20] and the cumulative effect of all H···I interactions can be generally correlated with the extent of perovskite sheet penetration (see Table 1). Hydrogen bonding to the axial iodides should have little impact on the band gap because they do not contribute to either the valence or conduction bands. Similarly, hydrogen bonding to equatorial iodides in structures with no out-of-plane distortion will largely interact with the electron density of the I p_z orbitals, which have π character with respect to the Sn orbitals, and thus they also have no character in the valence or conduction bands. However, in structures with out-of-plane distortions, hydrogen bonding to the equatorial iodides will perturb the Sn−I bonding. Any charge-transfer component to the hydrogen bonding will slightly stabilize the top of the valence band and thus may be responsible for the increased exciton energies of alkylammonium salts **13** and **14**, where interdigitation of the alkyl chains causes the out-of-plane distortions that allow substantial penetration of the ammonium head into the perovskite sheet. By contrast, adding steric bulk around the ammonium head as in the 2-substituted PEA cations **10**−**12** forces out-of-plane distortions but prevents penetration of the ammonium head into

(21) Xu, Z.; Mitzi, D. B. *Inorg. Chem.* **2003**, *42*, 6589.
(22) Ishihara, T. In *Optical Properties of Low-Dimensional Materials*; Ogawa, T., Kanemitsu, Y., Eds.; World Scientific: Singapore, 1995; pp 288−339.

the perovskite sheet, thus preventing a significant impact of the hydrogen bonding on the valence band. The deep penetration of the ammonium head observed for the TMAEA salt may also be responsible for its exciton energy being high relative to that expected for the extent of distortion. A series of higher-level calculations, beyond the scope of this paper, should be performed to examine the possible effects of the dielectric environment and hydrogen bonding on the electronic band structure of these materials.

Conclusion

The band gap as well as the bandwidth of the valence and conduction bands of the $(RNH_3)_2SnI_4$ hybrid semiconductor perovskites can be subtly influenced by variation in the structural requirements of the organic cation. Specifically, the Sn−I−Sn bond angle is shown to be a dominant structural factor influencing the electronic structure of these materials; the equatorial Sn−I bond distances exhibit a secondary influence. The current calculations indicate the possibility of tuning the band gap by as much as 1 eV using the steric impact of the organic cation on the inorganic framework. To date, most of the layered perovskites have been synthesized with organic species bound to the small, relatively high charge density ammonium headgroup. To accommodate the charge density of this small cation, the hybrid perovskite structure generally collapses with an in-plane twist distortion of the perovskite sheet. This distortion decreases the width of both the valence and conduction bands and increases the band gap. By contrast, to accommodate the larger size (lower charge density) of, for example, a trimethylammonium headgroup, an out-of-plane distortion of the tin iodide lattice is observed. The latter distortion primarily impacts the valence band because this distortion leaves one of the two dimensions of the conduction band effectively unperturbed. In cases where sterically demanding R groups are bound to the high-charge density ammonium head, an out-of-plane distortion is combined with the cationic head-driven in-plane distortion. However, these examples, again, demonstrate that the in-plane distortion has the greatest impact on the electronic structure. Therefore, to prepare hybrid perovskite materials with the smallest band gap and greatest width of the valence and conduction bands, it would be interesting to investigate hybrid materials prepared with sterically unencumbered templating cations whose head is better charge density matched with an ideal undistorted SnI_4^{2-} lattice.

Acknowledgment. The authors gratefully acknowledge the help of Prof. Z. Xu in the preparation of the data for Table 1. The work at NCSU was supported by NSF Grant DMR-0305086.

IC050244Q